

School of Integrated Circuits and Electronics, Beijing Institute of Technology, Beijing, China
Department of Radiology, Beijing Tiantan Hospital, Capital Medical University, Beijing, China

ARTICLE INFO

Article history:

Received 12 October 2021
Received in revised form 12 October 2022
Accepted 12 October 2022

Keywords:

Convolutional neural networks
diffusion magnetic resonance imaging
white matter

ABSTRACT

Convolutional neural networks (CNNs) are widely used in medical image analysis, especially in diffusion magnetic resonance imaging (dMRI) for white matter (WM) tractography.

The main challenge in dMRI tractography is the low signal-to-noise ratio (SNR) of the data, which leads to noisy and incomplete fiber reconstructions. In this paper, we propose a deep learning-based method for dMRI tractography. Our method consists of two main parts: a denoising network and a tractography network. The denoising network is designed to remove the noise from the dMRI data while preserving the underlying fiber structure. The tractography network is designed to reconstruct the fiber tracts from the denoised data. We evaluate our method on both simulated and real dMRI data. The results show that our method outperforms the state-of-the-art methods in terms of fiber reconstruction accuracy and completeness. Specifically, our method achieves a higher fiber reconstruction accuracy and a higher fiber reconstruction completeness compared to the state-of-the-art methods. This is because our method can effectively remove the noise from the dMRI data and reconstruct the fiber tracts more accurately and completely. Our method is a promising approach for dMRI tractography and can be applied to other medical image analysis tasks.

201 (, 2011).

regions
of interest () ()
200 (, 201)
201 (, 200)
201 (, 2020).

(, 2021).

(, 200).

k- (, 2011)
(, 201) (, 201).
, convolutional neural networks ()
(, 2020) (, 201)
(, 2020).

2021 (Lu et al., 2021).

(Lu et al., 2021)

2

2. Methods

2.1. Problem formulation and classic fine-tuning

2

(Lu et al., 2021)

$$\begin{aligned}
 & \mathcal{M} \quad \mathcal{M}, \\
 & \mathcal{M} \quad \mathcal{M} \\
 & L \quad \mathcal{M} \quad L \quad \mathcal{M} \quad \theta, \theta, \\
 & \theta. \quad \mathcal{M} \quad \mathcal{M} \\
 & \mathbf{F} \quad \mathbf{X} \quad \mathbf{X} \quad \theta \\
 & \mathbf{F} = f(\mathbf{X}; \theta), \tag{1}
 \end{aligned}$$

$$\mathbf{F} \quad \mathbf{P} \quad \mathbf{P} \\
 \mathbf{F} \quad L \quad L$$

2 (Lu et al., 2021)

$$\begin{aligned}
 & g(\mathbf{F}; \theta) \quad g(\mathbf{F}; \theta) \quad \theta \quad \theta, r, \dots \\
 & \mathbf{P} = g(\mathbf{F}; \theta) = g(f(\mathbf{X}; \theta); \theta), \quad \mathbf{P}
 \end{aligned}$$

$$p_{\rightarrow j}^v = \frac{1}{1 + \exp(-b_j + \sum_{i=1}^M w_{ij}h_{\rightarrow i}^v)}, \quad (1)$$

$$\mathbf{P}_{\rightarrow}^v = (p_{\rightarrow 1}^v, \dots, p_{\rightarrow N}^v)^T, \quad (2)$$

$$\mathbf{P}_{\rightarrow}^v = \sigma(\mathbf{W}\mathbf{H}^v + \mathbf{b}), \quad (3)$$

$$\mathbf{W} = \begin{bmatrix} w_{11} & \dots & w_{1M} \\ \vdots & \ddots & \vdots \\ w_{N1} & \dots & w_{NM} \end{bmatrix}, \quad \mathbf{b} = b_1, \dots, b_N^T. \quad (4)$$

$$\mathbf{H}^v = \tilde{\mathbf{W}} \tilde{\mathbf{F}}^v + \mathbf{b}, \quad \tilde{\mathbf{F}}^v = f(\mathbf{X}; \theta), \quad \theta = \{\mathbf{W}, \mathbf{b}\}$$

$$\mathbf{P}_{\rightarrow}^v = \sigma(\mathbf{W}(\tilde{\mathbf{W}} \tilde{\mathbf{F}}^v + \mathbf{b}) + \mathbf{b}) = \sigma(\mathbf{W}\tilde{\mathbf{W}} \tilde{\mathbf{F}}^v + \mathbf{W}\mathbf{b} + \mathbf{b}). \quad (5)$$

$$\mathbf{W} \leftarrow \mathbf{W}\tilde{\mathbf{W}}, \quad \mathbf{b} \leftarrow \mathbf{W}\mathbf{b} + \mathbf{b}. \quad (6)$$

2.3. A better implementation with warmup

$$\mathbf{W}' = \mathbf{W}\tilde{\mathbf{W}}, \quad \mathbf{b}' = \mathbf{W}\mathbf{b} + \mathbf{b}. \quad (7)$$

$$\mathbf{P}_{\rightarrow}^v = \sigma(\mathbf{W}'\tilde{\mathbf{F}}^v + \mathbf{b}'). \quad (8)$$

$$\theta = \{\mathbf{W}', \mathbf{b}'\}, \quad \theta \in \mathcal{M}, \quad \theta = \{\mathbf{W}, \mathbf{b}\} \in \mathcal{M}$$

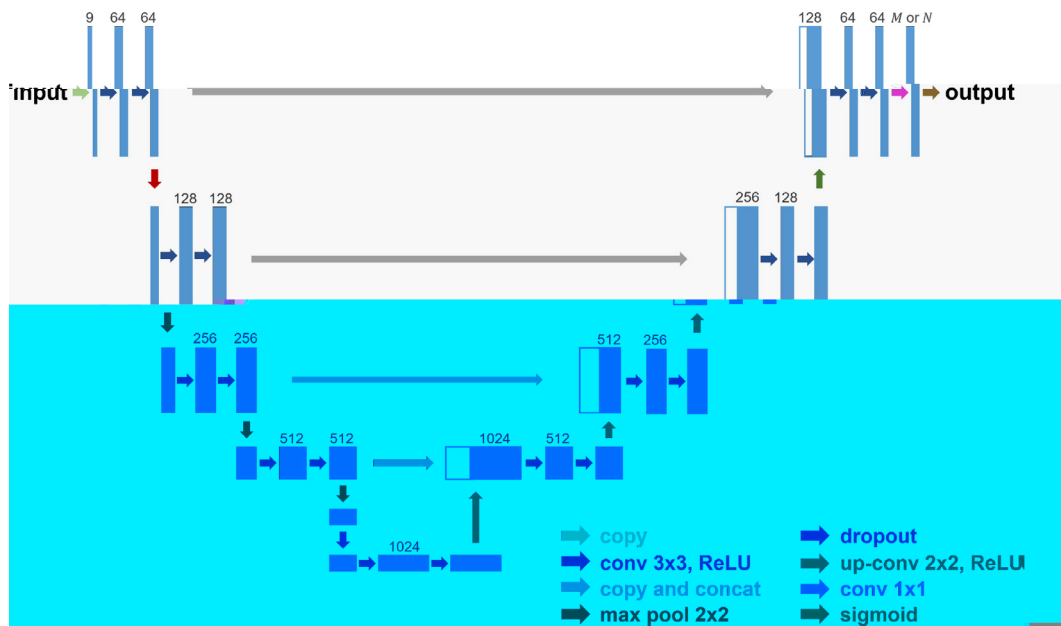


Fig. 1.

$$\mathbf{M} = \begin{bmatrix} \mathbf{M}_1 & \mathbf{M}_2 & \dots & \mathbf{M}_N \end{bmatrix} \quad (10)$$

$$\mathbf{M}_i = \begin{bmatrix} \mathbf{M}_{i1} & \mathbf{M}_{i2} & \dots & \mathbf{M}_{iK} \end{bmatrix} \quad (11)$$

$$\mathbf{M}_{ij} = \begin{bmatrix} \mathbf{M}_{ij1} & \mathbf{M}_{ij2} & \dots & \mathbf{M}_{ijK} \end{bmatrix} \quad (12)$$

where \mathbf{M}_i is the i -th slice of the multi-shell multi-tissue constrained spherical deconvolution (MSMT-CSD) tensor, \mathbf{M}_{ij} is the j -th slice of the i -th slice of the MSMT-CSD tensor, and \mathbf{M}_{ijl} is the l -th slice of the j -th slice of the i -th slice of the MSMT-CSD tensor.

where \mathbf{M}_i is the i -th slice of the MSMT-CSD tensor, \mathbf{M}_{ij} is the j -th slice of the i -th slice of the MSMT-CSD tensor, and \mathbf{M}_{ijl} is the l -th slice of the j -th slice of the i -th slice of the MSMT-CSD tensor.

where \mathbf{M}_i is the i -th slice of the MSMT-CSD tensor, \mathbf{M}_{ij} is the j -th slice of the i -th slice of the MSMT-CSD tensor, and \mathbf{M}_{ijl} is the l -th slice of the j -th slice of the i -th slice of the MSMT-CSD tensor.

where \mathbf{M}_i is the i -th slice of the MSMT-CSD tensor, \mathbf{M}_{ij} is the j -th slice of the i -th slice of the MSMT-CSD tensor, and \mathbf{M}_{ijl} is the l -th slice of the j -th slice of the i -th slice of the MSMT-CSD tensor.

where \mathbf{M}_i is the i -th slice of the MSMT-CSD tensor, \mathbf{M}_{ij} is the j -th slice of the i -th slice of the MSMT-CSD tensor, and \mathbf{M}_{ijl} is the l -th slice of the j -th slice of the i -th slice of the MSMT-CSD tensor.

where \mathbf{M}_i is the i -th slice of the MSMT-CSD tensor, \mathbf{M}_{ij} is the j -th slice of the i -th slice of the MSMT-CSD tensor, and \mathbf{M}_{ijl} is the l -th slice of the j -th slice of the i -th slice of the MSMT-CSD tensor.

where \mathbf{M}_i is the i -th slice of the MSMT-CSD tensor, \mathbf{M}_{ij} is the j -th slice of the i -th slice of the MSMT-CSD tensor, and \mathbf{M}_{ijl} is the l -th slice of the j -th slice of the i -th slice of the MSMT-CSD tensor.

where \mathbf{M}_i is the i -th slice of the MSMT-CSD tensor, \mathbf{M}_{ij} is the j -th slice of the i -th slice of the MSMT-CSD tensor, and \mathbf{M}_{ijl} is the l -th slice of the j -th slice of the i -th slice of the MSMT-CSD tensor.

where \mathbf{M}_i is the i -th slice of the MSMT-CSD tensor, \mathbf{M}_{ij} is the j -th slice of the i -th slice of the MSMT-CSD tensor, and \mathbf{M}_{ijl} is the l -th slice of the j -th slice of the i -th slice of the MSMT-CSD tensor.

where \mathbf{M}_i is the i -th slice of the MSMT-CSD tensor, \mathbf{M}_{ij} is the j -th slice of the i -th slice of the MSMT-CSD tensor, and \mathbf{M}_{ijl} is the l -th slice of the j -th slice of the i -th slice of the MSMT-CSD tensor.

where \mathbf{M}_i is the i -th slice of the MSMT-CSD tensor, \mathbf{M}_{ij} is the j -th slice of the i -th slice of the MSMT-CSD tensor, and \mathbf{M}_{ijl} is the l -th slice of the j -th slice of the i -th slice of the MSMT-CSD tensor.

$$\mathbf{M} = \begin{bmatrix} \mathbf{M}_1 & \mathbf{M}_2 & \dots & \mathbf{M}_N \end{bmatrix} \quad (10)$$

$$\mathbf{M}_i = \begin{bmatrix} \mathbf{M}_{i1} & \mathbf{M}_{i2} & \dots & \mathbf{M}_{iK} \end{bmatrix} \quad (11)$$

$$\mathbf{M}_{ij} = \begin{bmatrix} \mathbf{M}_{ij1} & \mathbf{M}_{ij2} & \dots & \mathbf{M}_{ijK} \end{bmatrix} \quad (12)$$

where \mathbf{M}_i is the i -th slice of the multi-shell multi-tissue constrained spherical deconvolution (MSMT-CSD) tensor, \mathbf{M}_{ij} is the j -th slice of the i -th slice of the MSMT-CSD tensor, and \mathbf{M}_{ijl} is the l -th slice of the j -th slice of the i -th slice of the MSMT-CSD tensor.

where \mathbf{M}_i is the i -th slice of the MSMT-CSD tensor, \mathbf{M}_{ij} is the j -th slice of the i -th slice of the MSMT-CSD tensor, and \mathbf{M}_{ijl} is the l -th slice of the j -th slice of the i -th slice of the MSMT-CSD tensor.

where \mathbf{M}_i is the i -th slice of the MSMT-CSD tensor, \mathbf{M}_{ij} is the j -th slice of the i -th slice of the MSMT-CSD tensor, and \mathbf{M}_{ijl} is the l -th slice of the j -th slice of the i -th slice of the MSMT-CSD tensor.

where \mathbf{M}_i is the i -th slice of the MSMT-CSD tensor, \mathbf{M}_{ij} is the j -th slice of the i -th slice of the MSMT-CSD tensor, and \mathbf{M}_{ijl} is the l -th slice of the j -th slice of the i -th slice of the MSMT-CSD tensor.

where \mathbf{M}_i is the i -th slice of the MSMT-CSD tensor, \mathbf{M}_{ij} is the j -th slice of the i -th slice of the MSMT-CSD tensor, and \mathbf{M}_{ijl} is the l -th slice of the j -th slice of the i -th slice of the MSMT-CSD tensor.

where \mathbf{M}_i is the i -th slice of the MSMT-CSD tensor, \mathbf{M}_{ij} is the j -th slice of the i -th slice of the MSMT-CSD tensor, and \mathbf{M}_{ijl} is the l -th slice of the j -th slice of the i -th slice of the MSMT-CSD tensor.

where \mathbf{M}_i is the i -th slice of the MSMT-CSD tensor, \mathbf{M}_{ij} is the j -th slice of the i -th slice of the MSMT-CSD tensor, and \mathbf{M}_{ijl} is the l -th slice of the j -th slice of the i -th slice of the MSMT-CSD tensor.

where \mathbf{M}_i is the i -th slice of the MSMT-CSD tensor, \mathbf{M}_{ij} is the j -th slice of the i -th slice of the MSMT-CSD tensor, and \mathbf{M}_{ijl} is the l -th slice of the j -th slice of the i -th slice of the MSMT-CSD tensor.

where \mathbf{M}_i is the i -th slice of the MSMT-CSD tensor, \mathbf{M}_{ij} is the j -th slice of the i -th slice of the MSMT-CSD tensor, and \mathbf{M}_{ijl} is the l -th slice of the j -th slice of the i -th slice of the MSMT-CSD tensor.

where \mathbf{M}_i is the i -th slice of the MSMT-CSD tensor, \mathbf{M}_{ij} is the j -th slice of the i -th slice of the MSMT-CSD tensor, and \mathbf{M}_{ijl} is the l -th slice of the j -th slice of the i -th slice of the MSMT-CSD tensor.

where \mathbf{M}_i is the i -th slice of the MSMT-CSD tensor, \mathbf{M}_{ij} is the j -th slice of the i -th slice of the MSMT-CSD tensor, and \mathbf{M}_{ijl} is the l -th slice of the j -th slice of the i -th slice of the MSMT-CSD tensor.

where \mathbf{M}_i is the i -th slice of the MSMT-CSD tensor, \mathbf{M}_{ij} is the j -th slice of the i -th slice of the MSMT-CSD tensor, and \mathbf{M}_{ijl} is the l -th slice of the j -th slice of the i -th slice of the MSMT-CSD tensor.

where \mathbf{M}_i is the i -th slice of the MSMT-CSD tensor, \mathbf{M}_{ij} is the j -th slice of the i -th slice of the MSMT-CSD tensor, and \mathbf{M}_{ijl} is the l -th slice of the j -th slice of the i -th slice of the MSMT-CSD tensor.

2.5. Backbone network for WM tract segmentation

The backbone network for WM tract segmentation is designed to process the input data and generate the output. It consists of several stages of feature extraction and refinement.

The input data is processed through a series of convolutional layers. The first stage involves a 3x3 convolution with ReLU activation, followed by a 2x2 max pooling operation. This is followed by a series of 1x1 convolutions and dropout layers to refine the features.

The refined features are then processed through a series of up-convolutional layers (2x2) with ReLU activation, followed by a final 1x1 convolution and sigmoid activation to produce the output.

The output of the backbone network is used for WM tract segmentation, where the network identifies and segments the white matter tracts in the input data.

The network is trained using a multi-shell multi-tissue constrained spherical deconvolution (MSMT-CSD) method, which allows for the simultaneous estimation of multiple fiber orientations within each voxel.

The MSMT-CSD method is implemented using a constrained spherical deconvolution (CSD) algorithm, which ensures that the estimated fiber orientations are physically plausible and consistent with the underlying tissue structure.

The CSD algorithm is implemented using a series of spherical harmonics (SH) coefficients, which are used to represent the fiber orientations in a compact and efficient manner.

The SH coefficients are estimated using a series of least-squares minimization steps, which iteratively refine the fiber orientation estimates until convergence is reached.

The final output of the network is a set of segmented white matter tracts, which can be used for further analysis and visualization in medical image analysis.

The network is trained using a cross-entropy loss function, which measures the difference between the predicted and ground truth segmentations. The training process is optimized using an Adam optimizer.

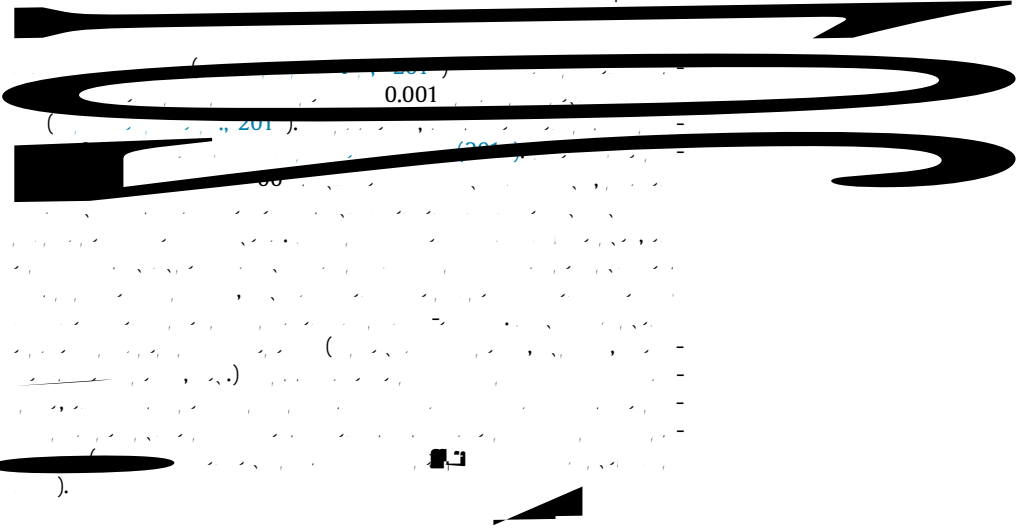
The network is evaluated using a series of metrics, including accuracy, precision, recall, and F1 score, to assess its performance on the WM tract segmentation task.

The results of the evaluation show that the network achieves high performance on the WM tract segmentation task, demonstrating its effectiveness in identifying and segmenting white matter tracts in medical images.

The network is implemented in Python using the PyTorch framework, and is available as an open-source project on GitHub.

Table 1

	12				
1					
2					
				10	
				11	
				12	



3. Results

(, 201-)

01 12 0 .0 201-

3.1. Data description and experimental settings

3.1.1. The HCP dataset

(, 201-)

2 0 (,

3.1.2. The private dataset

(Liu et al., 2021)

$(b = 1000, 2000, \dots, 10000 / 2^k), (k = 0, 1, \dots, 10)$

(201)

$0, 1, \dots, 20$

put28.3749.161.3d1 Tf 61.1749 614.9611 Tm [() TJ 0.0044 6.6]6F677.72 1 Tf 6.7.9701 [()05591 531.2791 Tm [(segmenting)] T447.98855677.72 1 T

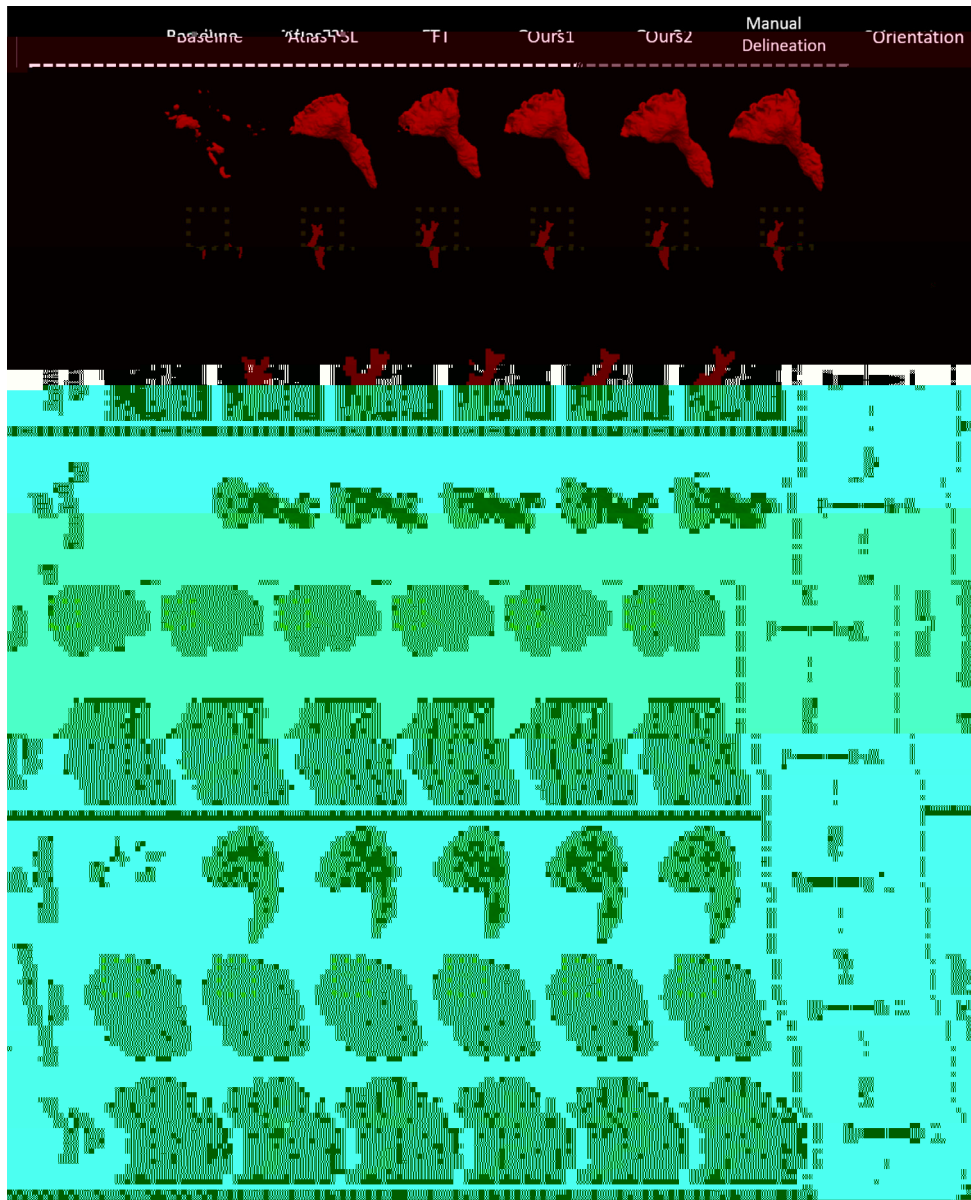


Fig. 2. Comparison of WM tract delineation results. The top row shows the 3D surface reconstructions of WM tracts. The middle four rows show the 2D cross-sections of WM tracts in axial, sagittal, coronal, and oblique planes. The bottom row shows the 2D cross-sections of WM tracts in the original MRI slices. The methods compared are Ground Truth, Ours1, Ours2, Manual Delineation, and Orientation. The results show that Ours1 and Ours2 provide more accurate and complete WM tract delineation compared to the other methods.

relative volume difference (RVD) (Liu et al., 2021),

$$RVD = \frac{|V_{\text{Ours}} - V_{\text{GT}}|}{V_{\text{GT}}} \quad (1)$$

where V_{Ours} and V_{GT} are the volumes of the WM tracts delineated by Ours and the Ground Truth, respectively. The RVD is used to evaluate the accuracy of the WM tract delineation. The lower the RVD, the more accurate the delineation. In this study, the RVD of Ours1 and Ours2 is significantly lower than that of the other methods, indicating that Ours1 and Ours2 provide more accurate WM tract delineation.

($p < 0.001$) ($d > 0.1$) ($d > 0.1$)

3.2.2. Impact of the number of training scans annotated for novel WM tracts

The impact of the number of training scans annotated for novel WM tracts on the performance of Ours1 and Ours2 is evaluated. The results show that the performance of Ours1 and Ours2 improves as the number of training scans increases. The RVD of Ours1 and Ours2 decreases as the number of training scans increases, indicating that more training scans lead to more accurate WM tract delineation.

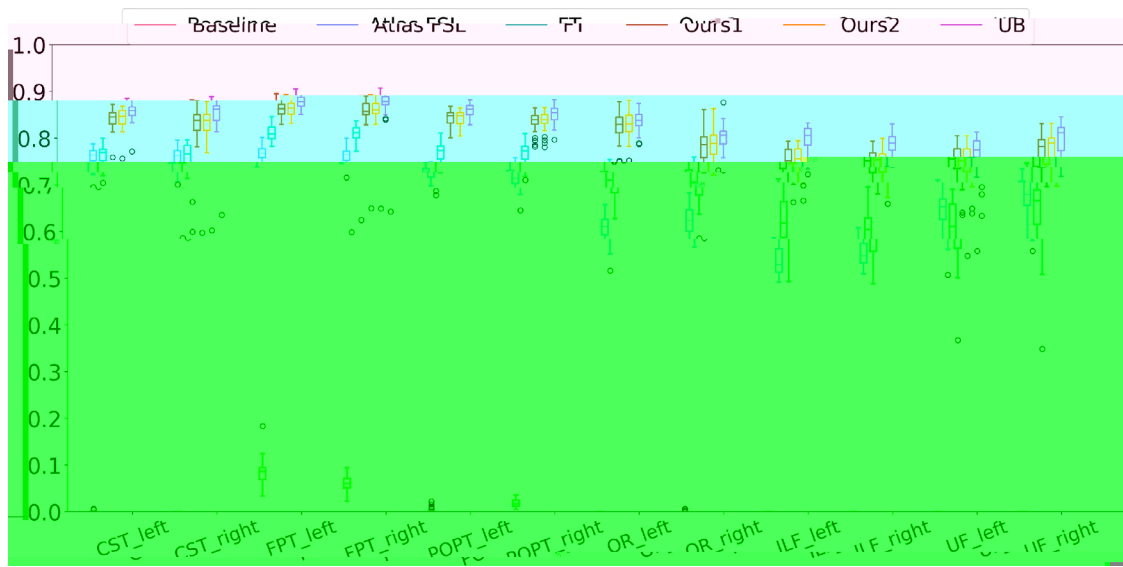


Fig. 3. Comparison of the performance of the proposed method with the baseline method and other methods in the 12 regions (1: 1, 2: 2).

Table 2

Region	Method 1			Method 2		
	d	p	t	d	p	t
CST_left	0.1	***	1.1	0.1	***	1.1
CST_right	0.1	***	1.1	0.1	***	1.1
FPT_left	0.1	***	1.1	0.1	***	1.1
FPT_right	0.1	***	1.1	0.1	***	1.1
POPT_left	0.1	***	1.1	0.1	***	1.1
POPT_right	0.1	***	1.1	0.1	***	1.1
OR_left	0.1	***	1.1	0.1	***	1.1
OR_right	0.1	***	1.1	0.1	***	1.1
ILF_left	0.1	***	1.1	0.1	***	1.1
ILF_right	0.1	***	1.1	0.1	***	1.1
UF_left	0.1	***	1.1	0.1	***	1.1
UF_right	0.1	***	1.1	0.1	***	1.1

Table 3

Method 1		Method 2	
d	p	d	p
0.1	0.0	0.1	0.0

Comparison of the performance of the proposed method with the baseline method and other methods in the 12 regions (1: 1, 2: 2). (***: $p < 0.001$, $d > 0.1$).

Table 4

		Baseline	Atlas FSL	FT	Ours1	Ours2	UB
1	d	0.000	0.1	0.0	0.777	0.784	0.2
	p	***	*	***	**	-	-
2	d	0.02	0.1	0.0	0.811	0.812	0.1
	p	***	*	***	**	-	-

Table 5

		Baseline	Atlas FSL	FT	Ours1	Ours2	UB
1	d	1.000	0.12	0.2	0.156	0.151	0.10
	p	***	*	***	**	-	-
2	d	0.1	0.1	0.1	0.129	0.131	0.10
	p	***	*	*	**	-	-

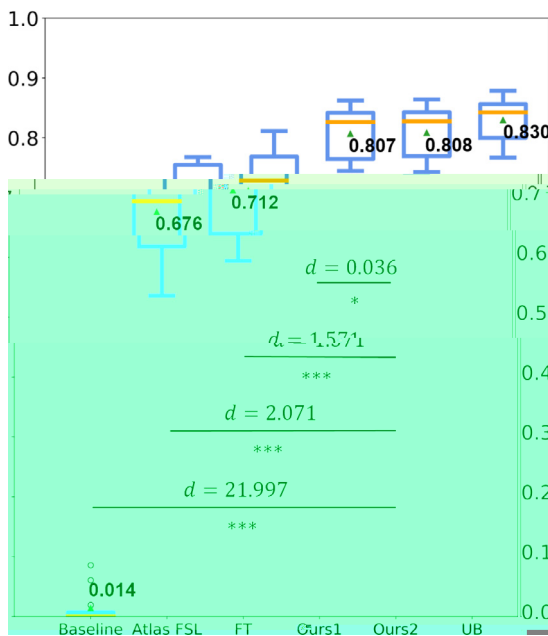


Fig. 4. Performance comparison of different methods. The y-axis represents the performance metric. The x-axis represents the methods. The values above the boxes indicate the median performance. The horizontal lines with brackets indicate the pairwise differences (d) and significance levels. (*p < .05, **p < .01, ***p < .001).

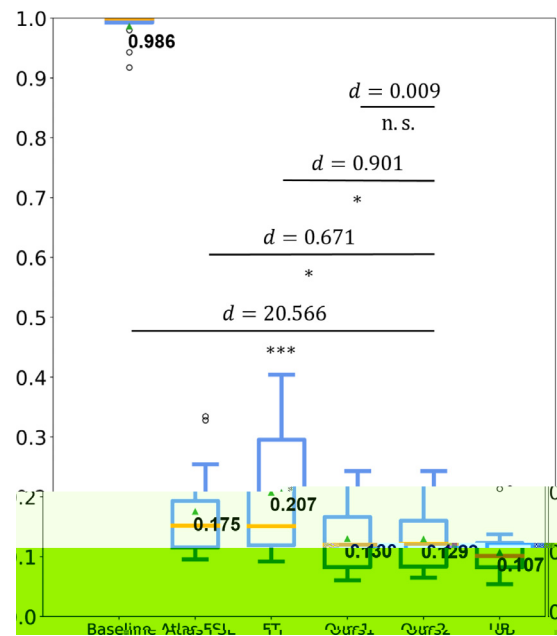


Fig. 5. Performance comparison of different methods. The y-axis represents the performance metric. The x-axis represents the methods. The values above the boxes indicate the median performance. The horizontal lines with brackets indicate the pairwise differences (d) and significance levels. (*p < .05, **p < .01, ***p < .001).

($d < 0.2$)

3.2.3. Segmentation performance with different selections of novel WM tracts

11

12

3.2.4. Impact of data quality

13

Table 7

Table 7: Comparison of the proposed method with other methods in terms of accuracy, precision, recall, and F1 score. The table is organized into three groups based on the number of classes (1, 2, and 3) and the number of samples (2 and 2+). The columns represent the methods: Proposed, DNN, and ResNet. The rows represent the metrics: Accuracy, Precision, Recall, and F1 score. The values are presented as mean ± standard deviation. The statistical significance is indicated by asterisks (*, **, ***). The p-value is also provided for each comparison.

Method	Metric	1			2			3		
		Proposed	DNN	ResNet	Proposed	DNN	ResNet	Proposed	DNN	ResNet
2	Accuracy	0.000	0.000	0.000	0.694	0.724	0.000	0.000	0.000	0.000
	d	1.0	1.1	1.0	0.0	-	-	0.0	0.0	0.0
	p	***	***	***	***	***	***	***	***	***
	p	0.000	0.000	0.000	0.758	0.764	0.000	0.000	0.000	0.000
2+	Accuracy	0.000	0.000	0.000	0.757	0.761	0.000	0.000	0.000	0.000
	d	1.0	1.0	1.0	0.0	-	-	0.0	0.0	0.0
	p	***	***	***	*	-	-	***	***	***
	p	0.000	0.000	0.000	0.000	0.000	0.000	0.000	0.000	0.000

Table 8

Table 8: Comparison of the proposed method with other methods in terms of accuracy, precision, recall, and F1 score. The table is organized into three groups based on the number of classes (1, 2, and 3) and the number of samples (2 and 2+). The columns represent the methods: Proposed, DNN, and ResNet. The rows represent the metrics: Accuracy, Precision, Recall, and F1 score. The values are presented as mean ± standard deviation. The statistical significance is indicated by asterisks (*, **, ***). The p-value is also provided for each comparison.

Method	Metric	1			2			3		
		Proposed	DNN	ResNet	Proposed	DNN	ResNet	Proposed	DNN	ResNet
2	Accuracy	1.000	0.22	1.0	0.258	0.213	0.1	1.0	1.0	1.0
	d	1.0	0.1	1.0	0.0	-	-	0.0	0.0	0.0
	p	***	*	***	***	***	***	***	***	***
	p	1.000	0.2	0.2	0.159	0.157	0.1	0.0	0.0	0.0
2+	Accuracy	1.000	0.2	0.2	0.183	0.176	0.1	1.0	1.0	1.0
	d	12.0	0.0	1.0	0.0	-	-	0.0	0.0	0.0
	p	***	***	***	*	-	-	***	***	***
	p	1.000	0.2	0.2	0.000	0.000	0.000	0.000	0.000	0.000

Table 9

Table 9: Comparison of the proposed method with other methods in terms of accuracy, precision, recall, and F1 score. The table is organized into three groups based on the number of classes (1, 2, and 3) and the number of samples (2 and 2+). The columns represent the methods: Proposed, DNN, and ResNet. The rows represent the metrics: Accuracy, Precision, Recall, and F1 score. The values are presented as mean ± standard deviation. The statistical significance is indicated by asterisks (*, **, ***). The p-value is also provided for each comparison.

Method	Metric	1			2			1+2			2+3		
		Proposed	DNN	ResNet	Proposed	DNN	ResNet	Proposed	DNN	ResNet	Proposed	DNN	ResNet
2	Accuracy	0.00	0.0	0.2	0.645	0.694	0.715	0.0	0.0	0.0	0.728	0.0	0.0
	d	1.11	2.1	2.121	1.2	0.0	0.2	1.0	1.0	1.0	-	-	-
	p	***	***	***	***	***	**	***	***	***	***	***	***
	p	0.1	0.2	0.0	0.398	0.326	0.305	0.0	0.0	0.0	0.277	0.0	0.0
2+	Accuracy	10.1	0.0	2.11	1.2	0.0	0.2	0.0	0.0	0.0	-	-	-
	d	10.1	0.0	2.11	1.2	0.0	0.2	0.0	0.0	0.0	-	-	-
	p	***	*	***	***	***	**	***	***	***	***	***	***
	p	0.00	0.10	0.0	0.667	0.712	0.732	0.0	0.0	0.0	0.743	0.0	0.0
3	Accuracy	0.0	0.2	0.0	0.358	0.294	0.275	0.0	0.0	0.0	0.252	0.0	0.0
	d	0.0	0.1	0.0	0.622	0.675	0.698	0.0	0.0	0.0	0.712	0.0	0.0
	p	0.0	0.1	0.0	***	***	***	***	***	***	***	***	***
	p	0.0	0.2	0.2	0.439	0.358	0.335	0.0	0.0	0.0	0.301	0.0	0.0

Table 10

Table 10: Comparison of the proposed method with other methods in terms of accuracy, precision, recall, and F1 score. The table is organized into three groups based on the number of classes (1, 2, and 3) and the number of samples (2 and 2+). The columns represent the methods: Proposed, DNN, and ResNet. The rows represent the metrics: Accuracy, Precision, Recall, and F1 score. The values are presented as mean ± standard deviation. The statistical significance is indicated by asterisks (*, **, ***). The p-value is also provided for each comparison.

Method	Metric	1			2			1+2			2+3		
		Proposed	DNN	ResNet	Proposed	DNN	ResNet	Proposed	DNN	ResNet	Proposed	DNN	ResNet
2	Accuracy	0.00	0.02	0.20	0.687	0.713	0.720	0.0	0.0	0.0	0.717	0.0	0.0
	d	0.0	0.2	0.0	0.344	0.286	0.284	0.0	0.0	0.0	0.280	0.0	0.0
	p	0.000	0.0	0.2	0.540	0.662	0.670	0.0	0.0	0.0	0.682	0.0	0.0
	p	0.0	0.0	0.2	0.538	0.366	0.359	0.0	0.0	0.0	0.346	0.0	0.0

()

Declaration of Competing Interest

The authors declare that they have no known competing financial interests or personal relationships that could have appeared to influence the work reported in this paper.

CRediT authorship contribution statement

Qi Lu: Conceptualization, Methodology, Software, Validation, Visualization, Writing - original draft, Writing - review & editing. Zhizheng Zhuo: Conceptualization, Methodology, Software, Validation, Visualization, Writing - original draft, Writing - review & editing. Yuxing Li: Conceptualization, Methodology, Software, Validation, Visualization, Writing - original draft, Writing - review & editing. Yanyun Duan: Conceptualization, Methodology, Software, Validation, Visualization, Writing - original draft, Writing - review & editing. Pinnan Yu: Conceptualization, Methodology, Software, Validation, Visualization, Writing - original draft, Writing - review & editing. Liying Qu: Conceptualization, Methodology, Software, Validation, Visualization, Writing - original draft, Writing - review & editing. Chuyang Ye: Conceptualization, Methodology, Software, Validation, Visualization, Writing - original draft, Writing - review & editing. Yaou Liu: Conceptualization, Methodology, Software, Validation, Visualization, Writing - original draft, Writing - review & editing.

Acknowledgments

This work was supported by the National Natural Science Foundation of China (12071404), the National Natural Science Foundation of China (12071404) & (12171404), the National Natural Science Foundation of China (12071404), the National Natural Science Foundation of China (12071404).

Appendix A. Segmentation accuracy of the proposed method achieved with and without TractMix for the HCP dataset

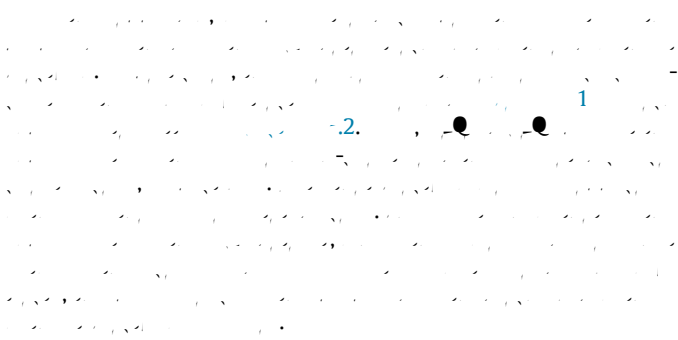


Table A:1

	1	2	1+	2+
●	0.11	0.12	0.12	0.12
●	0.0	0.0	0.0	0.0
●	0.2	0.2	0.2	0.2
●	0.21	0.21	0.21	0.21
●	0.	0.1	0.1	0.
●	0.	0.	0.	0.

References

1. Q. Lu, W. Liu, Z. Zhuo, et al., "TractMix: A novel tract-based method for brain white matter segmentation," *Medical Image Analysis*, vol. 79, p. 102454, 2022.

2. Q. Lu, W. Liu, Z. Zhuo, et al., "TractMix: A novel tract-based method for brain white matter segmentation," *Medical Image Analysis*, vol. 79, p. 102454, 2022.

3. Q. Lu, W. Liu, Z. Zhuo, et al., "TractMix: A novel tract-based method for brain white matter segmentation," *Medical Image Analysis*, vol. 79, p. 102454, 2022.

4. Q. Lu, W. Liu, Z. Zhuo, et al., "TractMix: A novel tract-based method for brain white matter segmentation," *Medical Image Analysis*, vol. 79, p. 102454, 2022.

2021. [https://doi.org/10.1016/j.mbs.2021.102454](#).

1020. [https://doi.org/10.1016/j.mbs.2021.102454](#).

2021. [https://doi.org/10.1016/j.mbs.2021.102454](#).